Spin polarization of Co(0001)/graphene junctions from first principles

2014 J. Phys.: Condens. Matter 26 104204

(http://iopscience.iop.org/0953-8984/26/10/104204)

IOP Publishing Journal of Physics: Condensed Matter
J. Phys.: Condens. Matter **26** (2014) 104204 (9pp) doi:10.1088/0953-8984/26/10/104204

Spin polarization of Co(0001)/graphene junctions from first principles

G M Sipahi[1,5], Igor Žutić[1], N Atodiresei[2], R K Kawakami[3] and P Lazić[4]

[1] Department of Physics, University at Buffalo, State University of New York, Buffalo, NY 14260, USA
[2] Peter Grünberg Institut and Institute for Advanced Simulation, , Forschungszentrum Jülich and JARA, D-52425 Jülich, Germany
[3] Department of Physics and Astronomy, University of California, Riverside, CA 92521, USA
[4] Rudjer Boskovic Institute, PO Box 180, Bijenička c. 54, 10 002 Zagreb, Croatia

E-mail: plazicx@gmail.com

Received 22 August 2013, revised 4 October 2013
Published 19 February 2014

Abstract
Junctions comprised of ferromagnets and nonmagnetic materials are one of the key building blocks in spintronics. With the recent breakthroughs of spin injection in ferromagnet/graphene junctions it is possible to consider spin-based applications that are not limited to magnetoresistive effects. However, for critical studies of such structures it is crucial to establish accurate predictive methods that would yield atomically resolved information on interfacial properties. By focusing on Co(0001)/graphene junctions and their electronic structure, we illustrate the inequivalence of different spin polarizations. We show atomically resolved spin polarization maps as a useful approach to assess the relevance of Co(0001)/graphene for different spintronics applications.

(Some figures may appear in colour only in the online journal)

1. Introduction

While the crucial importance of carbon in molecular electronics (moltronics) [1, 2] has been recognized for several decades, only more recently has it also become clear that a similar potential may arise for spintronics [3, 4]. One can also envision desirable materials and device properties emerging from the combination of moltronics and spintronics [5]. Perhaps the key push for carbon-based spintronics comes from graphene which, with many impressive breakthroughs in the past few years, has become one of the most versatile materials, holding promise for many new applications and for improving existing ones. Figure 1 illustrates the lattice structure of graphene with a two-atom unit cell which leads to two band crossings per Brillouin zone at the K and K′ points. The conduction and valence bands only touch at the charge neutrality points, forming Dirac cones with linear dispersion, while flat-band regions give rise to peaks in the density of states. Because of its two-dimensional nature and electronic structure graphene has interesting mechanical and electronic properties. Owing to the strong sp^2 in-plane bonding, graphene has structural stability and mechanical strength. Out-of-plane π states define the transport and binding properties of graphene. Some applications of graphene rely on its self-standing properties, such as DNA sequencing [6], while others inevitably include graphene deposited on a certain surface.

In spintronics a typical building block is comprised of ferromagnet/nonmagnet structures [7], so one of the key questions in graphene spintronics would be to develop a systematic understanding of ferromagnet/graphene (F/Gr) junctions, with both single and multi-layer graphene. Our theoretical goal, discussed in this work, focuses on developing *ab initio* studies to elucidate atomically resolved information for such junctions that would also apply to multi-layer graphene, predicted to give excellent spin filtering [8–11]. Traditionally, junctions with ferromagnets are used in spintronics to realize spin-valve structures and magnetoresistive effects [7], which have also been experimentally demonstrated employing graphene [12–17]. However, graphene spintronics may also offer other opportunities that are not limited to magnetoresistance for implementing magnetic sensing and information storage. In fact,

[5] On subbatical leave from: Instituto de Física de São Carlos, Universidade de São Paulo, Brazil.

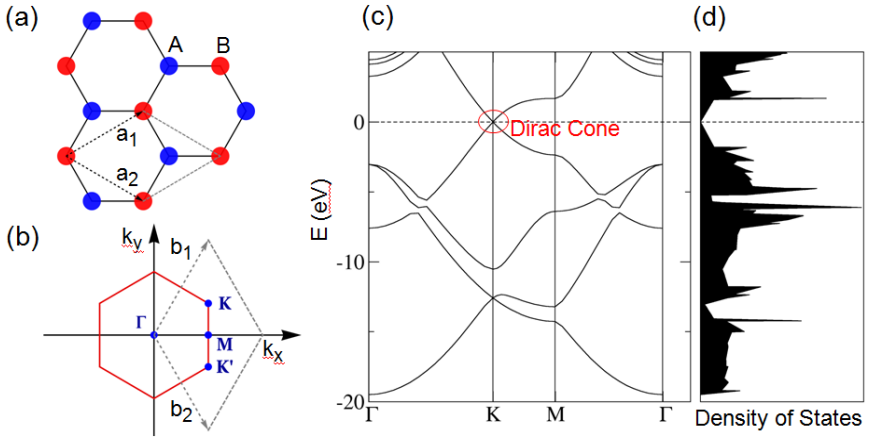

Figure 1. (a) The honeycomb lattice and (b) the corresponding Brillouin zone of graphene. (c) The band structure of graphene with a marked Dirac cone at the K point. (d) The density of states shows pronounced peaks, as expected from the flat-band regions in (c). The results (c) and (d) have been calculated from first principles using the same set of parameters as described later in the text.

experimental breakthroughs in F/Gr junctions have revealed a very effective method for room temperature spin injection [18] with record high values for spin accumulation [19]. Another desirable property of F/Gr junctions is that the graphene layer can be a suitable replacement for tunnel regions and provide robust spin injection in semiconductors [20] with desirable resistance values [21]. Despite being atomically thin, owing to sp^2 bonding, graphene can effectively prevent metallic ions from migrating from the F-region into the semiconductor, increasing the longevity of devices [20]. With the chemical inertness of graphene (the carbon atoms tend not to interact with out-of-plane atoms), there are fewer charge-traps leading to a dynamical response to spin injection free of charging-time delays, suggesting fast and stable operation [21].

One can then envision that such graphene-enhanced spin injection could enable a variety of other devices not limited to magnetoresistive effects, such as magnetologic gates [22, 23], spin interconnects [24], and spin lasers [25–28]. To highlight the optimization of novel spintronic devices through first-principles calculations, we briefly discuss an example of a spin laser, relying on spin injection to generate an imbalance of spin-up and spin-down carriers that leads to the emission of circularly polarized light [25, 29]. A simple analogy of water pumped into a bucket can already illustrate how such lasers work and qualitatively explain various experiments that confirm their improved operation, as compared to their conventional (spin-unpolarized) counterparts [26, 27, 30]. Water added to the bucket represents the injection of carriers into the laser, while the water coming out of the overfilled bucket corresponds to the emitted light through lasing. To consider the effect of spin injection and the net carrier spin polarization, we choose a bucket partitioned in half and each of the halves separately filled with hot and cold water, representing spin-up and spin-down carriers, respectively [25]. In an idealized case of an F/Gr spin injector providing, say, only spin-up carriers, this bucket analogy would tell us that only one half of the bucket needs to be filled for water to overflow and thus explain experiments showing that spin lasers can lase at a reduced injection intensity[6]. This threshold reduction can also be related to the improved dynamical properties of spin lasers, such as the enhanced bandwidth [31, 32]. On the other hand, the previously mentioned reduced number of charge-traps in F/Gr junctions could also enable the fabrication of spin injectors with fast spin modulation to achieve other advantages envisioned for spin lasers [25, 33].

With this motivation it should be clear that it is important to seek ferromagnetic surfaces which are suitable candidates for graphene adsorption. Ni(111) and Co(0001) have lattice constants close to that of graphene, which makes them suitable for *ab initio* studies, at a reasonable computational cost, by making them commensurate with the graphene lattice (or vice versa). The binding of graphene on metallic surfaces in general is an interesting topic which has been researched a lot recently [34–36, 38]. The possibility of hybridization of carbon orbitals with metallic states which cause a change in the graphene electronic structure and with the additional possibility of doping by adsorption or intercalation of additional chemical species is of great practical and technological interest. Furthermore, theoretical studies of graphene on metallic surfaces provide an excellent test bed for testing the accuracy of density functionals [39]. Graphene sheets and metallic surfaces both have relatively large polarizabilities which in combination with intermediate electron gas densities yield a significant nonlocal correlation interaction or van der Waals interaction (vdW). In particular, having more than one layer of graphene on top of one another creates a graphite structure in which the binding between the layers is exclusively of vdW nature. As mentioned previously, in multi-layer graphene one expects desirable spin filtering properties and thus the possibility to implement a highly efficient F/Gr spin injector [9]. This paper is organized as follows. First, we give the calculation details; next, we analyze the results of calculations looking at the geometry of

[6] An experimental demonstration of such lasing does not give an ideal reduction by a factor of two (to only fill one half of the bucket), since the injected carriers are not completely polarized and their degree of spin polarization could be further reduced through spin relaxation.

the system, band structure, density of states, charge transfer and hybridization analysis and nonlocal correlation binding energy; we also look at three different expressions for the polarization values as defined in [40] and compare them. Finally, we give conclusions.

2. Computational details

We have used Kohn–Sham density functional theory (DFT) [41] with the projector augmented wave method (PAW) [42, 43] as implemented in the VASP 5.1. computer code [44, 45]. Considering the light mass (the small atomic number) of carbon atoms and the spin–orbit gap which is only ∼24 μeV [46], it is accurate to perform nonrelativistic calculations[7]. We employed a plane wave cutoff of 500 eV and dipole correction [48, 49] in our calculations. All structures were allowed to relax until the atomic forces were below 1 meV Å^{-1}. We have used vdW-DF correlation [50, 51] with the optB88 exchange [39]. The nonlocal functional vdW-DF was selfconsistently implemented in VASP only recently [52] following the method of Román-Pérez and Soler [53], which makes its computational cost virtually identical to the cost of LDA/GGA (local density approximation/generalized gradient approximation) calculations. The Co(0001) slab was simulated by five layers of cobalt, all of which were allowed to relax, with an additional 22 Å of vacuum to avoid periodic image interaction. A k-point density of $9 \times 9 \times 1$ was used [54]. All calculations were spin polarized.

The reason for choosing optB88 is found in Mittendorfer *et al* [39] who have studied graphene on Ni(111) primarily by means of the random phase approximation (RPA) and exact exchange (EXX), which is about 200–300 times more costly than a GGA or vdW-DF type of calculation. The authors have used those results to find the type of exchange which is best suited for use with vdW-DF nonlocal correlation. Because of the very delicate interplay of charge transfer and vdW interaction the Ni(111)–Gr system was a very good reference system. The optB88 exchange in combination with vdW-DF reproduced the RPA–EXX curve very well and agreed well with the experimental results. Graphene on Co(0001) is in this respect similar to the Ni(111)–Gr system, i.e. there is a strong interaction, visible in the charge rearrangement and the change of the band structure, and yet a relatively weak adsorption is found. It should be mentioned that in an earlier paper [55] graphene on Ni(111) and Co(0001) was studied by the same method, i.e. RPA and EXX, and it was concluded that vdW-DF is inaccurate in the description of covalent bonds—which is not entirely correct[8]. The vdW-DF is by no means inaccurate in the description of the covalent bonds. It is exactly the idea of the vdW-DF functional that it is *seamless*—i.e. it should be able to describe any type of bonding accurately—from pure physisorption to strong chemisorption [56, 57]; however, the absolutely best choice of the exchange part for the vdW-DF type functional is still under discussion [58].

[7] In contrast, with compounds comprised of heavier elements the inclusion of spin–orbit coupling in *ab initio* studies can be particularly important [47].

[8] The authors of [55] give a correct conclusion in the reference section stating that vdW-DF is very sensitive to choice of the exchange functional, i.e. the final positions of the atoms are very sensitive to this. However, in the main text of [55] there is a different statement that vdW-DF has problems with describing the covalent bonding, which is not correct.

3. Results

3.1. Geometry of the system, binding energy, magnetic moments

To make the graphene unit cell commensurate with the Co(0001) we have scaled the graphene lattice constant ($a =$ 2.46 Å) to fit the Co one ($a = 2.49$ Å). The approach of adjusting the graphene lattice constant is more common in the literature [35, 39, 55]; however, one can also choose to adjust the metal lattice constant [34]. We believe that the latter approach is more physical, but we chose to change the graphene lattice constant in order to be able to compare our results with the results of others. The choice of which of the lattice constants is changed can have a significant influence on the results and it is known that for the case of the Cu(111) surface the binding strongly depends on this choice [55]. In reality, graphene often compensates for the lattice mismatch with the substrate over longer distances, usually followed by buckling of the graphene and creation of moiré patterns [59]. Calculation of such large cells is sometimes possible, but at a very large computational cost [36]. Even for the frequently used approach of considering a simplified lattice matched structure between Co and graphene that we employed here to reduce the computational complexity, one can estimate some influence of imperfections that could also modify our results for the calculated spin polarizations. For example, it is known that nanoscale charge puddles form in graphene [37] which lead to a substrate-dependent spatial variation of the chemical potential that we can model by a rigid shift in the electronic structure and the effective spin polarization. Meanwhile, in the case of a BN substrate this shift corresponds to only ∼10 meV; for SiO_2 it is considerably larger at ∼100 meV [37].

If not specified otherwise, all results are for the functional with vdW-DF correlation and optB88 exchange. We have tested three high symmetry positions of the carbon atoms in the unit cell: TOP–FCC, TOP–HCP and FCC–HCP. The TOP–FCC position is shown in figure 2.

The energies of the TOP–FCC and TOP–HCP structures are virtually identical, TOP–FCC being just slightly lower. The FCC–HCP structure is the highest in energy—102 meV higher than the other two. The distance from the C1 carbon atom to the Co atom below is 2.154 Å, which is close to the experimental value [60], and the binding energy is 77 meV per carbon atom, in very good agreement with the result of RPA–EXX calculation [55]. The PBE [61] calculation at the same geometry of the system gives 5 meV/C atom of repulsive interaction.

To further illustrate our approach, in table 1 we give magnetic moments for the different atoms, both for a pure Co(0001) surface and for one with graphene attached to it. We can better understand the computational slab used in table 1

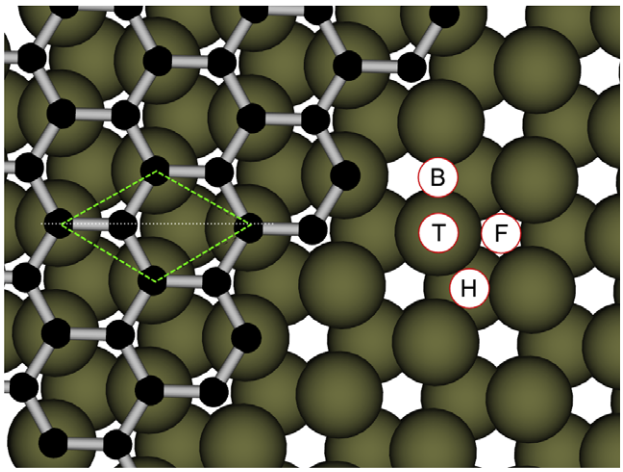

Figure 2. The Co(0001) surface with graphene adsorbed at the TOP–FCC position—top view. The carbon atoms are black and the cobalt atoms are brown. The unit cell is denoted by a dashed green line. The dotted white line shows the plane along which the cuts for the charge transfer and nonlocal binding energy are displayed in subsequent figures. For clarity, the right part of the figure shows only the cobalt atoms with the corresponding labels marking the high symmetry positions on the surface: F—FCC hollow, H—HCP hollow, T—TOP, B—bridge.

Table 1. The magnetic moment of a given atom in μ_B, for a pure Co(0001) surface (first row) and for the graphene adsorbed on the surface (second row). For reference, the magnetic moment obtained from a Co bulk calculation is 1.58 μ_B. The carbon atom C1 is the one at the TOP position, i.e. directly above the Co atom (see figure 2).

Co5	Co4	Co3	Co2	Co1	C1	C2
1.68	1.60	1.54	1.58	1.65		
1.68	1.61	1.54	1.54	1.50	−0.04	0.04

by recalling figure 2. The carbon atom C1 is at the TOP (T) position, directly above the cobalt atom Co1 in the first layer. On the other hand, the cobalt atom Co2 in the second layer is at the HCP (H) hollow position, in the center of the C-atom ring, with no carbon atom directly above it. As we will see, this inequivalence of the two environments for the Co1 and Co2 atoms will also lead to their distinct bonding and spin polarization properties. The carbon atom C2 is at the FCC (F) hollow position, with no Co atom in the layer just below it, making it thus inequivalent to the C1 atom.

3.2. Electronic structure

Since cobalt is a ferromagnet all quantities are shown for the minority and majority spin channels. The calculated density of states (DOS) is given in figure 3 while the band structure is shown in figure 4.

From the calculated band structure we conclude that the interaction between the graphene and the substrate is substantial—large enough to destroy the structure of the Dirac cone in both spin channels. In the majority spin channel a gap is opened between the apex points of the Dirac cones, at the K point in the Brillouin zone, and the states from both

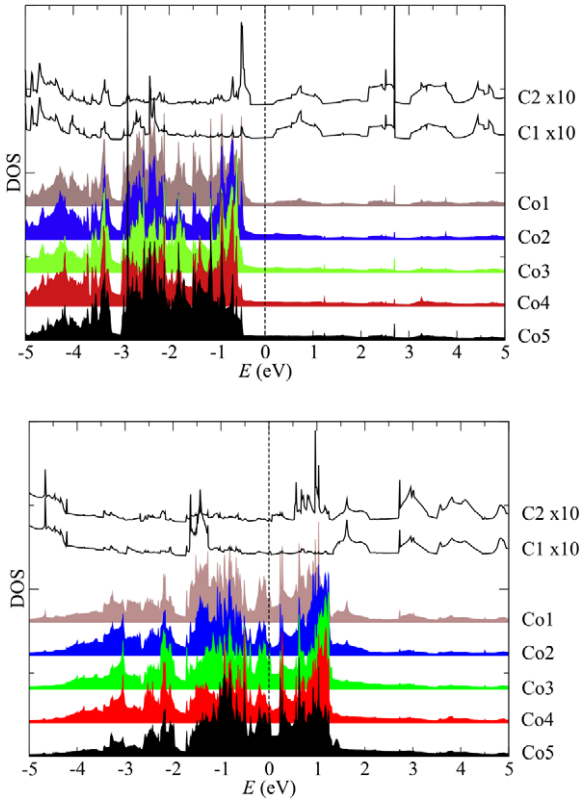

Figure 3. The atom-projected density of states (DOS). The data for each atom are shifted along the y-axis for clarity. The majority (upper panel) and minority (lower panel) spin channels are shown. The values for carbon atoms are scaled by a factor of 10. In all the graphs the energy is measured with respect to the Fermi energy.

sides of the gap are largely located in the graphene layer. The other spin channel has mostly metallic d-states around the K point in the Brillouin zone with a somewhat larger band gap in that region. Following the band structure lines of the free standing graphene along with the thicker lines of the system (projection onto the carbon atoms' orbitals) one can see how the graphene bands have hybridized with the Co(0001) states, especially around the Fermi level. In order to see the nature of the hybridization in section 3.3 we show the charge transfer plots.

3.3. Charge transfer

To understand the hybridization and the nature of the interaction in the F/Gr junction, which is already hinted at in figure 4, we plot the charge transfer in figure 5.

The charge transfer is defined as the difference in charge density between the system (graphene adsorbed on Co(0001)) and its parts at the exactly same positions as they have in the system (i.e. the surface and the graphene). In figure 5 we see how the inequivalent cobalt atoms Co1 and Co2 (recall also figure 2) reveal very different amounts of charge transfer. From the shapes of the charge depletion (blue) and charge accumulation (red) regions, we conclude that the carbon atoms at the TOP positions have accumulated charge into the p_z orbital. The charge mostly comes from the d-orbital of the

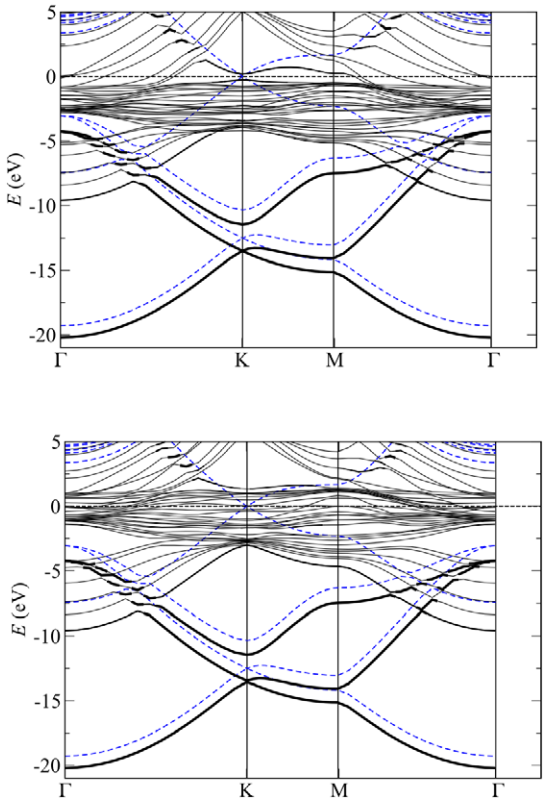

Figure 4. The band structure along the high symmetry lines of the Brillouin zone for majority (top) and minority (bottom) spin channels. The thickness of the lines is proportional to the localization of the eigenstate on the carbon atom (i.e. proportional to the projection onto carbon atomic orbitals). The blue dashed lines represent the band structure of the freestanding graphene.

underlying cobalt atom. The graphene attains a slight n-doping in this process, but we cannot interpret this charge transfer as a covalent bonding. Typically, a covalent bond contains a shared charge that has accumulated in the region between the bonded atoms. From the semilocal binding energy calculations it turns out that this charge rearrangement brings little or no bonding at all. This means that the largest part of the bonding energy is in the nonlocal correlation interaction which we visualize next. The nonlocal correlation interaction was introduced in the vdW-DF functional originally to capture the van der Waals interaction; however, it was introduced in a seamless fashion so that it remains valid regardless of whether the system is vdW or chemically bonded, or something in between those two extremes—which is the case here. Graphene on Ni(111) is very similar in that respect, and the term coined to describe such a system [39] is *strong interaction and weak adsorption*, meaning that there is a strong charge rearrangement at distances typical for chemical bonding, giving rise to strong hybridization of the states, but giving no binding in the semilocal functionals. The binding comes from the nonlocal correlation interaction at scales typical of a chemical bond and is in total relatively weak (around 100 meV/atom). There are also strongly chemically bound systems, involving again carbon atoms, where exactly this nonlocal correlation interaction at chemical bond length scales plays a crucial role—the most famous one being the *CO puzzle* [57] where that relatively small contribution is essential for site adsorption preference.

3.4. Nonlocal binding energy density

Following the definition of the nonlocal correlation binding energy in the vdW-DF functional [50] we can write the following expression:

$$\begin{aligned} E_{\mathrm{c}}^{\mathrm{NL}} &= \tfrac{1}{2}\iint \mathrm{d}\boldsymbol{r}\,\mathrm{d}\boldsymbol{r}'\, n(\boldsymbol{r})\phi(\boldsymbol{r},\boldsymbol{r}')n(\boldsymbol{r}') \\ &= \int \mathrm{d}\boldsymbol{r}\, n(\boldsymbol{r})\left[\tfrac{1}{2}\int \mathrm{d}\boldsymbol{r}'\,\phi(\boldsymbol{r},\boldsymbol{r}')n(\boldsymbol{r}')\right] \\ &= \int \mathrm{d}\boldsymbol{r}\, n(\boldsymbol{r})\epsilon_{\mathrm{c}}^{\mathrm{NL}}(\boldsymbol{r}) \\ &= \int \mathrm{d}\boldsymbol{r}\, e_{\mathrm{c}}^{\mathrm{NL}}(\boldsymbol{r}). \end{aligned} \tag{1}$$

This equation allows us to define the quantity $e_{\mathrm{c}}^{\mathrm{NL}}$ as a nonlocal correlation energy density. It is somewhat complicated to interpret a 3D visualization of such a quantity, since it shows an energy density at a given point which is a consequence of the interaction of the density at that point with all the other points in space (one should use a 6D space for a proper visualization). However, with some effort one can follow such images. Namely, the vdW-DF functional is based on the two contributions to the correlation energy. One

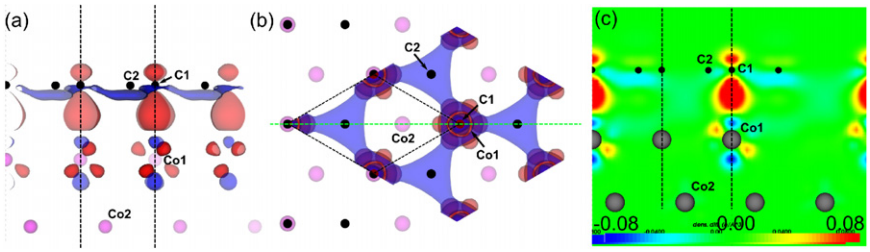

Figure 5. The charge rearrangement (difference of the charge densities of the system and its parts) near the corresponding carbon and cobalt atoms. Isosurfaces of values 0.03 (red) and −0.03 (blue) e Å^{-3} are shown using side (a) and top (b) views. The plane cutting through the unit cell denoted by the broken green line in (b) (and also marked by the white dotted line in figure 2), is shown in (c) to represent the charge transfer. (c) The color range from blue to red corresponds to values from −0.08 to 0.08 e Å^{-3}. The charge density is repeated throughout several unit cells—a single unit cell boundary is marked with black dashed lines in (a)–(c).

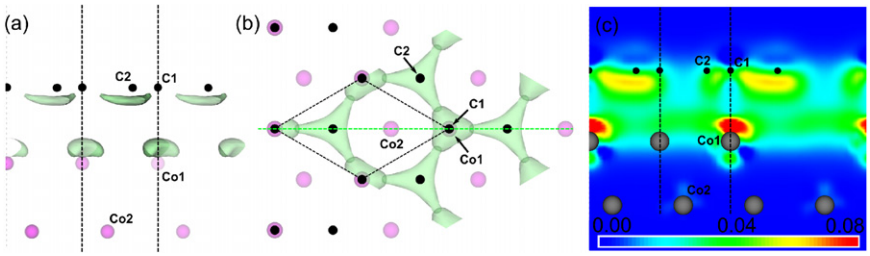

Figure 6. The nonlocal binding energy density near the corresponding carbon and cobalt atoms. An isosurface of value 60 meV Å^{-3} is shown using side (a) and top (b) views. (c) The plane cutting through the unit cell is spanning the color range from 0 (blue) to 80 (red) meV Å^{-3}. The plane cutting is denoted by the broken green line in (b) (and also marked by the white dotted line in figure 2). The nonlocal binding energy density is repeated throughout several unit cells—a single unit cell boundary is marked with black dashed lines in (a)–(c).

is an LDA correlation—which covers for the contribution of the correlation energy of the homogeneous electron gas—both local and nonlocal because the LDA is an analytical solution to the problem of the energy of a homogeneous electron gas. The remaining nonlocal double spatial integral, given in equation (1), is an additional contribution to the inhomogeneous deviation in density. Consequently, very close points in space will not have a large mutual nonlocal correlation energy contribution because typically such points in space are of similar density—which is covered by the LDA part of the functional (not shown). Therefore the most prominent contributions to the nonlocal binding energy density (which is again calculated as the difference of the energy density of the system and its parts) will appear in parts of the system which are brought closer together so that they interact via vdW. Namely, the electron gas at the bottom side of the graphene and the electron gas at the top side of the Co(0001) will interact with each other in a nonlocal way producing the largest contributions to the nonlocal binding, as shown in figure 6.

From the visualization of the nonlocal binding energy we conclude that this energy is relatively small per point, but is spread over a large area (volume). Thus, its total contribution to the binding energy is considerable, yet completely invisible for the local or semilocal functionals. We also note that the distribution of the nonlocal binding energy anticorrelates with the charge transfer, i.e. the regions in which charge is depleted are the ones that bring the major part of the nonlocal binding energy. The discussion of this phenomena is beyond the scope of this paper. Since it is not possible to generate images of the nonlocal binding energy from the VASP code we have used the JuNoLo code for that purpose [62]. One can explicitly show that the nonlocal binding energy stems from the interaction between the region around the graphene and the region on the Co surface, rather than from just one of these regions, by limiting the range of the interaction in equation (1) as was done in [57, 63].

3.5. Spin polarization

For many spintronic devices the key figure of merit is expressed in terms of the appropriate spin polarization [7]. However, an important consideration is to identify which specific polarization should be considered relevant: different experimental techniques can lead to very different spin polarizations, even for a uniform bulk material. To illustrate some of the subtleties, we recall a particularly simple implementation of the spin-valve effect in a magnetic tunnel junction with a nonmagnetic tunnel barrier, dating back to the Jullière model [64], with the tunneling magnetoresistance (TMR) expressed as [7, 64]

$$\mathrm{TMR} = \frac{2P_{\mathrm{L}}P_{\mathrm{R}}}{1 - P_{\mathrm{L}}P_{\mathrm{R}}}, \tag{2}$$

where $P_{\mathrm{L,R}}$ are polarizations commonly taken to be the spin-resolved densities of states in the left and right ferromagnets, respectively. Specifically, a figure of merit for a given ferromagnet could then be considered to be the DOS spin polarization at the Fermi level ($E = 0$),

$$P_N = \frac{N_\uparrow - N_\downarrow}{N_\uparrow + N_\downarrow}. \tag{3}$$

However, various concerns can be invoked against this interpretation, even when a more realistic transport description is not considered [65]. While it may appear from equations (2) and (3) that a spin polarization is a robust quantity for a given material, such as Co or Fe, a dramatic increase of the TMR was demonstrated with conventional ferromagnetic electrodes by simply replacing an Al_2O_3 barrier with MgO [11, 66, 67]. The same approach to enhance the TMR could be attributed to spin filtering also predicted in multi-layer graphene [9]. Moreover, P_N in equation (3) is generally not related to transport properties. Instead, as suggested by Mazin [40], it would be more relevant to consider a different effective polarization,

$$\mathrm{P}_{Nv^\alpha} = (\langle Nv^\alpha\rangle_\uparrow - \langle Nv^\alpha\rangle_\downarrow)/(\langle Nv^\alpha\rangle_\uparrow + \langle Nv^\alpha\rangle_\downarrow), \tag{4}$$

where the angular brackets denote performing the corresponding Fermi surface average. $\alpha = 1$ or P_{Nv} applies to ballistic transport, while $\alpha = 2$ or P_{Nv^2} yields the current polarization in the diffusive or tunneling regime [40].

We have used the expressions in equations (3) and (4) to calculate, from first principles, a different spin polarization for the Co(0001)/graphene junction. We chose a suitable way to represent the atomically- and energy-resolved spin polarization in figure 7, previously introduced for a Ni(111)/graphene junction [68]. The energy-resolved information about the spin

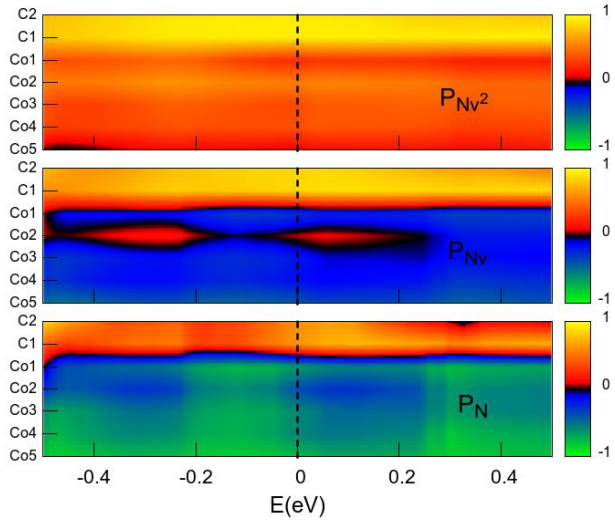

Figure 7. The spin polarization as defined in equations (3) and (4). The labels on the left show the atoms of the system, i.e. the Co slab and graphene layer. The color scale represents the span in polarization from the value −1 (green) to the value 1 (yellow).

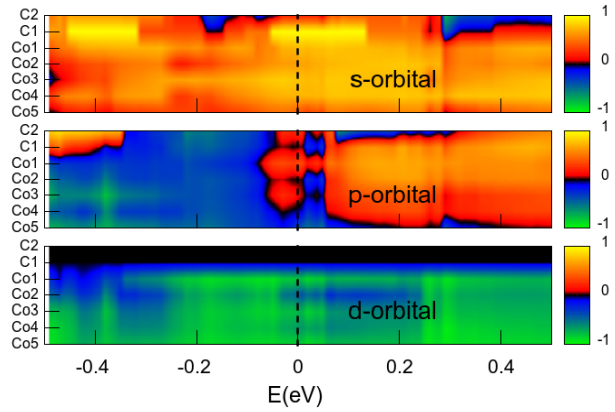

Figure 8. The simple polarization calculated from the DOS only, equation (3), and resolved spatially over the atoms, and over the symmetry of the atomic orbitals.

polarization can be useful to infer a possible bias-dependence of the spin injection, which can be present even in a free electron DOS, if a tunnel barrier is added [69]. We also provide additional information about the DOS spin polarization in figure 8 by showing its projections onto atomic orbitals.

From the polarization images several conclusions follow. The polarization for the Co region looks very different depending on which formula is used to calculate it, while in the graphene part it is not so sensitive. The reason for this is the same as Mazin's original argument for Ni: in the Co region there are d-bands (heavy, small Fermi velocity) and s- and p-bands (light, large Fermi velocity). Figure 8 presents the projected orbital polarizations. Joint analysis of figures 7 and 8 shows that the small polarization in Co from equation (4) is a result of the cancelation of the contributions of the d and p, s orbitals. It also shows that the higher mobility of the s and p orbitals is responsible for the large P_{Nv^2} polarization.

A closer look at figure 7 reveals that the P_{Nv} polarization, which has a modest value on cobalt atoms, can even change its sign from Co1 to Co2, for example at the Fermi level $E = 0$. To better understand this seemingly peculiar behavior, we recall that in figure 2 the local environments are inequivalent for these two atomic sites. Furthermore, as we have shown in figure 5, the charge transfer also differs significantly: at atom Co1 it is very strong, while it is almost negligible at Co2. This inequivalence of the two Co atoms implies different bonding to C atoms which should also be reflected in different s-, p- and d-orbital projections, as shown in figure 8. For example, we see a strong change in the d-orbital contribution. Its projection on Co1 is highly polarized (∼−1, green), but the Co2 projection is modest (∼−0.25, blue). If we then also add the s- and p-projection contributions (both positive at $E = 0$ and similar for both Co1 and Co2), we can confirm the figure 7 results: P_{Nv} for Co1 will be slightly negative (the positive s- and p-parts are not strong enough to overcome a very negative d-part), while Co2 will be slightly positive (positive s- and p-parts will dominate).

An analogous analysis and the use of different orbital contributions in figure 8 could also be applied to better understand the three different types of spin polarization in the region of the interfacial graphene. While we see that going from P_N to P_{Nv^2} will decrease the relative contribution of d orbitals and thus increase the corresponding spin polarization, in all three cases there is a similar and rather weak energy-dependence.

4. Conclusion

In this work we have used first-principles calculations to study the structural, electronic, and spin-dependent properties of ferromagnet/graphene junctions. We have emphasized the inequivalence of different spin polarizations and, by presenting atomically and energy-resolved maps, provided an effective way to analyze their relevance for different spintronic applications. For example, we can infer possible bias-dependence and transport properties, proximity effects, and a spin injection efficiency that can be expressed through various spin polarizations [7]. While we have focused on a specific Co(0001)/graphene system, one can envision many other material candidates that could be explored within a similar computational framework. In fact there is a wealth of other graphene-like 2D systems in which van der Waals interactions hold the key to their interlayer binding [70].

Even though our motivation was to provide a simple and cost-effective *ab initio* approach to study graphene systems, there are no fundamental obstacles to enhancing the complexity of the underlying theoretical description and including other relevant considerations. For example, one could use a larger computational cell and relax the assumption of lattice matching between the graphene and the ferromagnet. The inclusion of van der Waals interactions naturally provides a framework to study multi-layer graphene systems expected to yield highly effective spin filtering [9, 11, 10].

Acknowledgments

We thank H Dery, I I Mazin and L J Sham for valuable discussions. This work was supported by the US ONR, NSF-NRI NEB 2020, SRC, NSF-ECCS, FAPESP (No. 2011/19333-4), CNPq (No. 246549/2012-2) and the Center for Computational Research, University at Buffalo.

References

[1] Mirkin C A and Ratner M A 1992 *Annu. Rev. Phys. Chem.* **43** 719
[2] Reed M A 1999 *Proc. IEEE* **87** 652
[3] Józsa C and van Wees B J 2011 *Handbook of Spin Transport and Magnetism* ed E Y Tsymbal and I Žutić (New York: CRC Press)
[4] Seneor P, Dlubak B, Martin M-B, Anane A, Jaffres H and Fert A 2012 *MRS Bull.* **37** 1245
[5] Raman K V *et al* 2013 *Nature* **493** 509
[6] Garaj S, Hubbard W, Reina A, Kong J, Branton D and Golovchenko J A 2010 *Nature* **467** 190
[7] Žutić I, Fabian J and Das Sarma S 2004 *Rev. Mod. Phys.* **76** 323
Fabian J, Matos-Abiague A, Ertler C, Stano P and Žutić I 2007 *Acta Phys. Slovaca* **57** 565
[8] Mavropoulos P, Papanikolaou N and Dederichs P H 2000 *Phys. Rev. Lett.* **85** 1088
[9] Karpan V M, Giovannetti G, Khomyakov P A, Talanana M, Starikov A A, Zwierzycki M, van den Brink J, Brocks G and Kelly P J 2007 *Phys. Rev. Lett.* **99** 176602
[10] Maassen J, Ji W and Guo H 2011 *Nano Lett.* **11** 151
[11] Saha K K, Blom A, Thygesen K S and Nikolić B K 2012 *Phys. Rev.* B **85** 184426
[12] Hill W, Geim A K, Novoselov K S, Schedin F and Blake P 2006 *IEEE Trans. Magn.* **42** 2694
[13] Tombros N, Józsa C, Popinciuc M, Jonkman H T and van Wees B J 2007 *Nature* **448** 571
[14] Cho S, Chen Y-F and Fuhrer M S 2007 *Appl. Phys. Lett.* **91** 123105
[15] Nishioka M and Goldman A M 2007 *Appl. Phys. Lett.* **90** 252505
[16] Ohishi M, Shiraishi M, Nouchi R, Nozaki T, Shinjo T and Suzuki Y 2007 *Japan. J. Appl. Phys.* 2 **46** L605
[17] Wang W H, Pi K, Li Y, Chiang Y F, Wei P, Shi J and Kawakami R K 2008 *Phys. Rev.* B **77** 020402(R)
[18] Han W, Pi K, McCreary K M, Li Y, Wong J J I, Swartz A G and Kawakami R K 2010 *Phys. Rev. Lett.* **105** 167202
Han W, McCreary K M, Pi K, Wang W H, Li Y, Wen H, Chen J R and Kawakami R K 2012 *J. Magn. Magn. Mater.* **324** 369
[19] Neumann I, Costache M V, Bridoux G, Sierra J F and Valenzuela S O 2013 *Appl. Phys. Lett.* **103** 112401
[20] van 't Erve O M J, Friedman A L, Cobas E, Li C H, Robinson J T and Jonker B T 2012 *Nature Nanotechnol.* **7** 737
[21] Dery H 2012 *Nature Nanotechnol.* **7** 692
[22] Dery H, Wu H, Ciftcioglu B, Huang M, Song Y, Kawakami R, Shi J, Krivorotov I, Žutić I and Sham L J 2012 *IEEE Trans. Electron Devices* **59** 259
Dery H *et al* 2011 *Proc. SPIE* **8100** 81000W
[23] Dery H, Dalal P, Cywinski L and Sham L J 2007 *Nature* **447** 573
[24] Dery H, Song Y, Li P and Žutić I 2011 *Appl. Phys. Lett.* **99** 082502
[25] Lee J, Oszwałdowski R, Gøthgen C and Žutić I 2012 *Phys. Rev.* B **85** 045314
[26] Holub M, Shin J, Saha D and Bhattacharya P 2007 *Phys. Rev. Lett.* **98** 146603
[27] Iba S, Koh S, Ikeda K and Kawaguchi H 2011 *Appl. Phys. Lett.* **98** 08113
[28] Gerhardt N C, Li M Y, Jähme H, Höpfner H, Ackemann T and Hofmann M R 2011 *Appl. Phys. Lett.* **99** 151107
[29] Gøthgen C, Oszwałdowski R, Petrou A and Žutić I 2008 *Appl. Phys. Lett.* **93** 042513
[30] Rudolph J, Hägele D, Gibbs H M, Khitrova G and Oestreich M 2003 *Appl. Phys. Lett.* **82** 4516
[31] Lee J, Falls W, Oszwałdowski R and Žutić I 2010 *Appl. Phys. Lett.* **97** 041116
[32] Saha D, Basu D and Bhattacharya P 2010 *Phys. Rev.* B **82** 205309
[33] Boéris G, Lee J, Výborný K and Žutić I 2012 *Appl. Phys. Lett.* **100** 121111
[34] Brako R, Šokčević D, Lazić P and Atodiresei N 2010 *New J. Phys.* **12** 113016
[35] Vanin M, Mortensen J J, Kelkkanen A K, Garcia-Lastra J M, Thygesen K S and Jacobsen K W 2010 *Phys. Rev.* B **81** 081408
[36] Busse C *et al* 2011 *Phys. Rev. Lett.* **107** 036101
[37] Das Sarma S, Adam S, Hwang E H and Rossi E 2011 *Rev. Mod. Phys.* **83** 407
[38] Janthon P, Viñes F, Kozlov S M, Limtrakul J and Illas F 2013 *J. Chem. Phys.* **138** 244701
[39] Mittendorfer F, Garhofer A, Redinger J, Klimeš J, Harl J and Kresse G 2011 *Phys. Rev.* B **84** 201401(R)
[40] Mazin I I 1999 *Phys. Rev. Lett.* **83** 1427
[41] Kohn W and Sham L J 1965 *Phys. Rev.* **140** A1133
[42] Blochl P E 1994 *Phys. Rev.* B **50** 17953
[43] Kresse G and Joubert D 1999 *Phys. Rev.* B **59** 1758
[44] Kresse G and Hafner J 1993 *Phys. Rev.* B **47** 558
[45] Kresse G and Furthmüller J 1996 *Phys. Rev.* B **54** 11169
[46] Gmitra M, Konschuh S, Ertler C, Ambrosch-Draxl C and Fabian J 2009 *Phys. Rev.* B **80** 235431
[47] Makinistian L, Faiz M M, Panguluri R P, Balke B, Wurmehl S, Felser C, Albanesi E A, Petukhov A G and Nadgorny B 2013 *Phys. Rev* B **87** 220402(R)
[48] Neugebauer J and Scheffler M 1992 *Phys. Rev.* B **46** 16067
[49] Bengtsson L 1999 *Phys. Rev.* B **59** 12301
[50] Dion M, Rydberg H, Schröder E, Langreth D C and Lundqvist B I 2004 *Phys. Rev. Lett.* **92** 246401
[51] Dion M, Rydberg H, Schröder E, Langreth D C and Lundqvist B I 2005 *Phys. Rev. Lett.* **95** 109902
[52] Klimeš J, Bowler D R and Michaelides A 2011 *Phys. Rev.* B **83** 195131
[53] Román-Pérez G and Soler J M 2009 *Phys. Rev. Lett.* **103** 096102
[54] Monkhorst H J and Pack J D 1976 *Phys. Rev.* B **13** 5188
[55] Olsen T, Yan J, Mortensen J J and Thygesen K S 2011 *Phys. Rev. Lett.* **107** 156401
[56] Lazić P, Atodiresei N, Caciuc V, Brako R, Gumhalter B and Blügel S 2012 *J. Phys.: Condens. Matter* **24** 424215
[57] Lazić P, Alaei M, Atodiresei N, Caciuc V, Brako R and Blügel S 2010 *Phys. Rev.* B **81** 045401
[58] Klimeš J, Bowler D R and Michaelides A 2010 *J. Phys.: Condens. Matter* **22** 022201
[59] Murata Y, Petrova V, Kappes B B, Ebnonnasir A, Petrov I, Xie Y-H, Ciobanu C V and Kodambaka S 2010 *ACS Nano* **4** 6509

[60] Eom D, Prezzi D, Rim K T, Zhou H, Lefenfeld M and Flynn S 2009 *Nano Lett.* **9** 2844
[61] Perdew J P, Burke K and Ernzerhof M 1996 *Phys. Rev. Lett.* **77** 3865
[62] Lazić P, Atodiresei N, Alaei M, Caciuc V, Blügel S and Brako R 2010 *Comput. Phys. Commun.* **181** 371
[63] Berland K and Hyldgaard P 2013 *Phys. Rev.* B **87** 205421
[64] Maekawa S and Shinjo T (ed) 2002 *Spin Dependent Transport in Magnetic Nanostructures* (New York: Taylor and Francis)
[65] Belaschenko K D and Tsymbal E Y 2011 *Handbook of Spin Transport and Magnetism* ed E Y Tsymbal and I Žutić (New York: CRC Press)
[66] Parkin S S P, Kaiser C, Panchula A, Rice P, Samant M and Yang S-H 2004 *Nature Mater.* **3** 862
[67] Yuasa S, Nagahama T, Fukushira A, Suzuki Y and Ando K 2004 *Nature Mater.* **3** 868
[68] Lazić P, Sipahi G M, Kawakami R K and Žutić I 2013 Preprint
[69] Monsma D J, Marcus C M, Narayanamurti V and Tinkham M 2005 *Phys. Rev. Lett.* **94** 196601
[70] Geim A K and Grigorieva I V 2013 *Nature* **499** 419